galaxies

MDPI

Article

Conical Stream of the Two-Sided Jets in NGC 4261 over the Range of 10^3–10^9 Schwarzschild Radii

Satomi Nakahara [1,2,*], Akihiro Doi [1,2], Yasuhiro Murata [1,2], Kazuhiro Hada [3], Masanori Nakamura [4] and Keiichi Asada [4]

1 Department of Space and Astronautical Science, The Graduate University for Advanced Studies, 3-1-1 Yoshinodai, Chuou-ku, Sagamihara, Kanagawa 252-0222, Japan; akihiro.doi@vsop.isas.jaxa.jp (A.D.); murata@vsop.isas.jaxa.jp (Y.M.)

2 The Institute of Space and Astronautical Science, Japan Aerospace Exploration Agency, 3-1-1 Yoshinodai, Chuou-ku, Sagamihara, Kanagawa 252-5210, Japan

3 National Astronomical Observatory of Japan, 2-21-1 Osawa, Mitaka, Tokyo 181-8588, Japan; kazuhiro.hada@nao.ac.jp

4 Institute of Astronomy & Astrophysics, Academia Sinica, P.O. Box 23-141, Taipei 10617, Taiwan; nakamura@asiaa.sinica.edu.tw (M.N.); asada@asiaa.sinica.edu.tw (K.A.)

* Correspondence: satomi.nakahara@vsop.isas.jaxa.jp; Tel.: +81-50-3362-2580

Academic Editors: Jose L. Gómez, Alan P. Marscher and Svetlana G. Jorstad
Received: 6 September 2016; Accepted: 14 December 2016; Published: 20 December 2016

Abstract: We report the jet width profile of of the nearby (∼30 Mpc) AGN NGC 4261 for both the approaching jet and the counter jet at radial distances ranging from ∼10^3–10^9 Schwarzschild radius (R_S) from the central engine. Our Very Large Array (VLA) and Very Long Baseline Array (VLBA) observations reveal that the jets maintain a conical structure on both sides over the range 10^3–10^9 R_S without any structural transition (i.e., parabolic to conical) like in the approaching jet in M87. Thus, NGC 4261 will provide a unique opportunity to examine the conical jet hypothesis in blazars, while it may require some additional consideration on the acceleration and collimation process in AGN jets.

Keywords: AGN jet; jet structure; VLBI observations

1. Introduction

The formation of relativistic jets in active galactic nuclei (AGNs) is a prominent topic in astrophysics, and recent observational studies on some nearby AGN jets have reported. The position of the central engine of M87—one of the nearest radio galaxies—has been determined by measuring shifts of the core position (Koñigl 1981 [1]; Lobanov 1998 [2]). with multi-frequency phase-referencing Very Long Baseline Interferometry (VLBI) observations (Hada et al. (2011) [3]). This result made it possible to investigate the radial profile of the physical parameters of an AGN jet. Nakamura and Asada (2012) [4] and Hada et al. (2013) [5] studied the radial profile of M87 jet width by taking into account the opacity shift of the VLBI core. Asada and Nakamura (2012) [6] discovered an enduring parabolic structure between a few 100 R_S and 10^5 R_S from the core, in addition to a transition into a conical structure beyond a distance of a location of ∼10^6 R_S, which is equivalent to the Bondi radius of M87. The revealed parabolic shape is compelling evidence that the jet collimates near the base of this jet. General relativistic magnetohydrodynamics (MHD) simulations (McKinney (2006) [7]) reproduce a parabolic collimation region by introducing external pressure, and a transition from parabolic to conical stream at ∼10^2 R_S. To study if such a transition is common in jets, more objects should be observed around the Bondi radii. The radial jet width profiles of 3C 84 (Nagai et al. (2014) [8]) and Cygnus A (Boccardi et al. (2016a, 2016b) [9,10]) have benn investigated recently; however, at distances remaining within the Bondi radius.

In this paper, we explore the jet width profile of NGC 4261 over the range 10^3–10^9 R_S, which contains the Bondi radius of this source (32 *pc*; Balmaverde, et al. (2008) [11] corresponding to 6.8×10^5 R_S). NGC 4261 (3C 270) is a nearby (31.6 Mpc; Tonry et al. (2000) [12]) Fanaroff-Riley Class I (FR-I) radio galaxy. NGC 4261 contains a central black hole with a mass of $(4.9 \pm 1.0) \times 10^8$ $M_\odot$ (Ferrarese et al. (1996) [13]) and nearly symmetric kiloparsec-scale two-sided jet structure (Birkinshaw and Davies (1985) [14]). This proximity and black hole mass yield a spatial scale, with 1 $milliarcsecond\,(mas) \sim 0.15\ pc \sim 3200\ R_S$, which provides an advantage for studying regions within 1 pc of the central engine. Furthermore, the position of the central engine of NGC 4261 has been determined by the phase-referencing VLBI technique; the origin of jet and the origin of the counter-jet are located at the same position, 82 ± 16 μas (projected) from the 43 GHz core, corresponding to 310 ± 60 R_S (deprojected) (Haga et al. (2015) [15]). This allows us to investigate the radial profile of the NGC 4261 jet width as a function of the (de-projected) distance along the jet from from the central engine, similarly to M87. Moreover, because of a large inclination angle ($i = 63°$; Piner et al. (2001) [16]), not only the approaching jet but also the counter jet can be imaged in the nuclear region, which is helpful for study of the jet formation.

2. Observations and Data Analysis

2.1. VLBA Data

We observed NGC 4261 with VLBA at four frequencies (1.4, 2.3, 5.0, and 8.4 GHz) on 3 July 2003, and at three frequencies (15, 22, and 43 GHz) on 6 June 2003. This is the same data presented in Haga et al. (2015) [15], which measured the core shift of NGC 4261 using the phase-referencing technique relative to the nearby radio source J1222+0413. Details of the observations and the data reduction processes are described in Haga et al. (2015) [15]. In the present paper, we remake self-calibrated images from these data sets, and measure the jet width at various distances. Although the images lose positional information from self-calibration, we apply the results from the core shift analysis (Haga et al. (2015) [15]), as we describe later in detail. The beam sizes and image qualities for the individual images are listed in Table 1.

Table 1. Image performance.

Telescope (1)	ν (GHz) (2)	I_{peak} (mJy/beam) (3)	σ (mJy/beam) (4)	θ_{maj} (mas) (5)	θ_{min} (mas) (6)
VLBA	1.4	47.4	0.5	8.9	4.5
	2.3	70.1	0.7	5.4	2.6
	5.0	117.1	0.6	2.5	1.2
	8.4	101.6	0.6	1.5	0.7
	15	113.4	0.7	0.9	0.4
	22	123.2	1.2	0.6	0.3
	43	72.9	0.9	0.3	0.2
VLA	1.4	159.2	0.4	1.7×10^3	1.4×10^3
	5.0	300.5	0.5	8.0×10^3	8.0×10^3

Columns are as follows: (1) Telescope; (2) Frequency; (3) Peak intensity; (4) Image RMS (Root Mean Square) noise; (5) The major axis size of the synthesized beam; (6) The minor axis size of the synthesized beam.

2.2. VLA Data

We also analyzed three archival VLA data sets (experiments AJ229, AP77, and AB376) from the data archive system of the National Radio Astronomy Observatory (NRAO). AJ229 was conducted on 15–16 April 1994 at 1.4 GHz (L-band). The VLA observed in A configuration with 27 antennas. Dual-circular polarization was received, covering a bandwidth of 3 MHz. The total on-source time on the target was approximately 5.5 h and 3C 286 was observed as the calibrator for 1 h. The data reduction

was performed in the standard manner using AIPS (Astronomical Image Processing System). We performed iterative de-convolution and self-calibration algorithms using Difmap to obtain a final image.

AP77 and AB376 were conducted on 23 April 1984 in C-configuration and 2 February 1986 in D-configuration, respectively, at 4.86 GHz (C-band). Dual-circular polarization was received, covering a bandwidth of 100 MHz. The two data sets were combined to obtain a final image, which is available on a website (http://www.slac.stanford.edu/teddy/Atlas/). The total on-source time on the target was approximately 0.5 h. The beam sizes and image qualities are listed in Table 1.

2.3. Jet Width Measurements

We performed a pixel-based analysis for all the data in the image plane. The jet width was measured using the AIPS task "slice ". Many nearby radio galaxies studied in recent other studies ([5,6,9]) show a double-ridge brightened jet structure; a double-Gaussian profile model is used for measuring their jet width. On the other hand, NGC 4261 shows a single-ridge jet structure, which extends almost due east–west (along position angle $PA \approx -90$ deg), as described in Figure 1, for example. Thus, we sliced each jet along the transverse direction ($PA \approx 180$ deg) and fitted a single-Gaussian profile model to the sliced intensity profile. The jet width θ_{jet} is determined by deconvolving it from the beam size; i.e., $\theta^2_{jet} = \theta^2_{fit} - \theta^2_{beam}$, where θ_{fit} and θ_{beam} are the full width at half maximum (FWHM) of fitted (Gaussian) function and the synthesized beam width at a position angle of 180 deg. The intensity slice at each distance was sampled at the Nyquist rate (1/2 FWHM of the synthesized beam). We measured the jet width for the approaching side every 1 mas, and on the counter-jet side every 0.2 mas from the radio core in the VLBA images in the region where the peak intensity is stronger than 3 σ. Note that not only the jet emission but also the lobe emission are apparent in the VLA image. We make a fit using two-Gaussians—one for the jet component and the other one for the lobe component—to avoid contamination from the lobe in the measurement of the jet width. The jet width was measured in the range over which the peak intensity of the jet is stronger than that of the lobe. Both sides of the jets on the VLA images were sliced every 10 arcsec from the radio core.

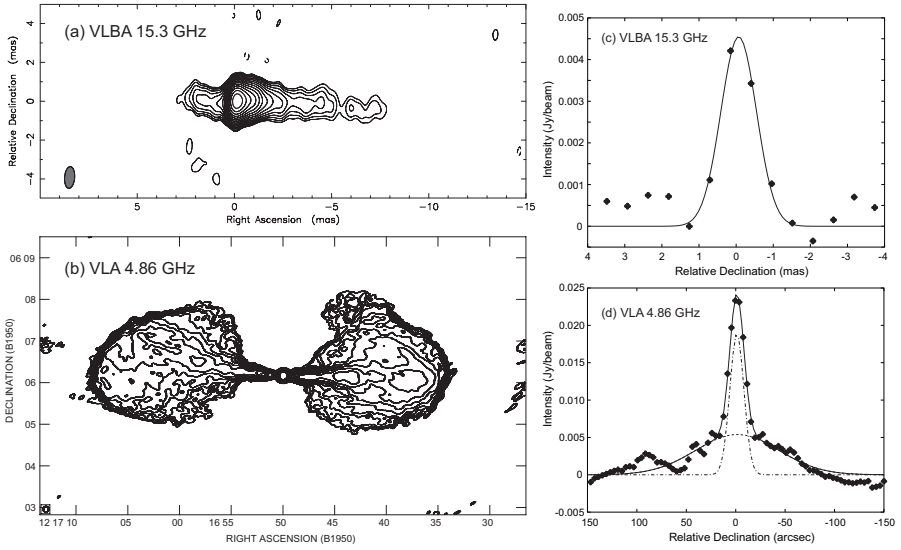

Figure 1. (**a**) VLBA image at 15 GHz. Contour levels are separated by factors of $\sqrt{2}$ beginning at the 3 sigma the RMS noise ($1\sigma = 0.358$ mJy beam^{-1}); (**b**) VLA image at 5 GHz. Contour levels are separated by factors of $\sqrt{2}$ beginning at 3 sigma the RMS noise ($1\sigma = 0.395$ mJy beam^{-1}); (**c**) Example of slice analysis of jet in VLBA image (15 GHz). Filled circles represent image intensity. Solid curve represents profile fitted using a Gaussian; (**d**) Example for slice analysis of jet in VLA image (5 GHz). Filled circles represent the image intensity. Dot–dashed curve represents a profile fitted to the jet component. Dashed curve represents a profile fitted to the lobe component. The solid curve represents a resultant profile of the fitted profiles of jet and lobe components.

We need the radial distance from the central engine to the location of the slice to calculate the radial profile of jet width for NGC 4261. The distance from the central engine to the radio core at each frequency was already determined using phase-referencing technique in Haga et al. (2015) [15]. Applying this result, we can calculate the radial distances from the central engine to the locations of our slice.

3. Results and Discussion

Figure 2 shows the radial profile of the NGC 4261 jet width as a function of the (de-projected) distance along jet (assuming the jet inclination angle $i = 63°$; Piner et al. (2001) [16]). The VLBA observations resolved the jet within the Bondi radius ($7 * 10^5$ R_s; dashed line in Figure 2), while the VLA observations imaged the jet beyond that distance. For the approaching jet, our (separate) power-law fitting of the measured jet collimation profile results in $a = 0.99 \pm 0.09$ (for the VLBA jet) and $a = 0.92 \pm 0.08$ (for the VLA jet) ($W_{\rm jet} \propto r^a$), respectively. Thus, the two fitting results are consistent within errors, indicating that the NGC 4261 jet structure has no transition across the Bondi radius, in contrast to the M87 jet profile (Asada and Nakamura (2012) [6]). Thus, we made a single fit to both data from the VLBA and the VLA; the results are $a = 1.06 \pm 0.01$ and $a = 1.06 \pm 0.01$ for the approaching jet (red line) and the counter jet (blue line), respectively. It is remarkable that both the jet and the counter jet sustain a conical structure over more than six orders of magnitude in distance. Furthermore, it is notable that the outflow is symmetric. These facts suggest: (1) the jet pressure is relatively too strong to be collimated by the external pressure; (2) the external pressure profile is symmetric without any transition at the Bondi radius or elsewhere. (3) We also found that the jets seem to converge upstream before reaching the black hole if we simply extrapolate the obtained jet profile toward the central engine. The jet profile may change further upstream, rather than over the range of our measurements.

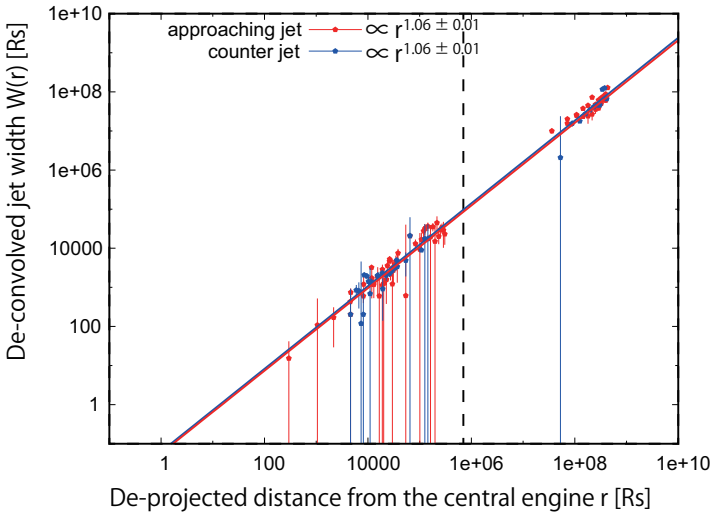

Figure 2. Radial profile of measured jet width for NGC 4261. The horizontal axis shows distance from the central engine, which is taken into account for the core shift effect. The vertical axis shows deconvolved jet width. Red and blue circles represent measurements of approaching and counter jets, respectively. The red and blue lines represent fitted profiles of approaching and counter jet widths, respectively. The dashed line indicates the Bondi radius of NGC 4261.

Acknowledgments: We thank C. C. Cheung for a high quality VLA image (5 GHz). S.N. was supported by THE JAPAN SCIENCE SOCIETY between April 2016 and March 2017.

Author Contributions: S.N. designed the study, and wrote the initial draft of the manuscript. All other authers contributed to analysis and interpretation of data, and assisted in the preparation of the manuscript. The final version of the manuscript was approved by all authors.

Conflicts of Interest: The authors declare no conflict of interest.

References

1. Konigl, A. Relativistic jets as X-ray and gamma-ray sources. *Astrophys. J.* **1981**, *243*, 700–709.
2. Lobanov, A.P. Ultracompact jets in active galactic nuclei. *Astron. Astrophys.* **1998**, *330*, 79–89.
3. Hada, K.; Doi, A.; Kino, M.; Nagai, H.; Hagiwara, Y.; Kawaguchi, N. An origin of the radio jet in M87 at the location of the central black hole. *Nature* **2011**, *477*, 185–187.
4. Nakamura, M.; Asada, K. The Parabolic Jet Structure in M87 as a Magnetohydrodynamic Nozzle. *Astrophys. J.* **2013**, *775*, 118.
5. Hada, K.; Kino, M.; Doi, A.; Nagai, H.; Honma, M.; Hagiwara, Y.; Giroletti, M.; Giovannini, G.; Kawaguchi, N. The Innermost Collimation Structure of the M87 Jet Down to $\sim$ 10 Schwarzschild Radii. *Astrophys. J.* **2013**, *775*, 70.
6. Asada, K.; Nakamura, M. The Structure of the M87 Jet: A Transition from Parabolic to Conical Streamlines. *Astrophys. J.* **2012**, *745*, L28.
7. McKinney, J.C. General relativistic magnetohydrodynamic simulations of the jet formation and large-scale propagation from black hole accretion systems. *Mon. Notic. Roy. Astron. Soc.* **2006**, *368*, 1561–1582.
8. Nagai, H.; Haga, T.; Giovannini, G.; Doi, A.; Orienti, M.; D'Ammando, F.; Kino, M.; Nakamura, M.; Asada, K.; Hada, K.; et al. Limb-brightened Jet of 3C 84 Revealed by the 43 GHz Very-Long-Baseline-Array Observation. *Astrophys. J.* **2014**, *785*, 53.
9. Boccardi, B.; Krichbaum, T.P.; Bach, U.; Mertens, F.; Ros, E.; Alef, W.; Zensus, J.A. The stratified two-sided jet of Cygnus A. Acceleration and collimation. *Astron. Astrophys.* **2016**, *585*, A33.
10. Boccardi, B.; Krichbaum, T.P.; Bach, U.; Bremer, M.; Zensus, J.A. First 3 mm-VLBI imaging of the two-sided jet in Cygnus A Zooming into the launching region. *Astron. Astrophys.* **2016**, *588*, L9.
11. Balmaverde, B.; Baldi, R.D.; Capetti, A.; Birkinshaw, M.; Davies, R.L. The accretion mechanism in low-power radio galaxies. *Astron. Astrophys.* **2008**, *486*, 119–130.
12. Tonry, J.L.; Blakeslee, J.P.; Ajhar, E.A.; Dressler, A. The Surface Brightness Fluctuation Survey of Galaxy Distances. II. Local and Large-Scale Flows. *Astrophys. J.* **2000**, *530*, 625–651.
13. Ferrarese, L.; Ford, H.C.; Jaffe, W. Evidence for a Massive Black Hole in the Active Galaxy NGC 4261 from Hubble Space Telescope Images and Spectra. *Astrophys. J.* **1996**, *470*, 444–459.
14. Birkinshaw, M.; Davies, R.L. The orientations of the rotation axes of radio galaxies. I - Radio morphologies of bright elliptical galaxies. *Astrophys. J.* **1985**, *291*, 32–44.
15. Haga, T.; Doi, A.; Murata, Y.; Sudou, H.; Kameno, S.; Hada, K. Determination of Central Engine Position and Accretion Disk Structure in NGC 4261 by Core Shift Measurements. *Astrophys. J.* **2015**, *807*, 15.
16. Piner, B.G.; Jones, D.L.; Wehrle, A.E. Orientation and Speed of the Parsec-Scale Jet in NGC 4261 (3C 270). *Astrophys. J.* **2001**, *122*, 2954–2960.